EUROPEAN JOURNAL OF MATERIALS SCIENCE AND ENGINEERING
Volume 10, Issue 2, 2025: 135-150 | www.ejmse.ro | ISSN: 2537-4338

DOI: 10.36868/ejmse.2025.10.02.135

INVESTIGATION OF MICROSTRUCTURE, CORROSION PERFORMANCE AND MECHANICAL PROPERTIES OF Mg- 5.45Zn-6.63Sn- 0.51Ca ALLOY

Md Nahid Rahman NAFI[1, *][0009-0008-5901-6820], Aninda Nafis AHMED[2] [0000-0003-2398-4025], Hossain M.M.A. RASHED[1][0000-0003-4781-8320]

[1]Department of Materials and Metallurgical Engineering, Bangladesh University of Engineering and Technology, Dhaka 1000, Bangladesh
[2]Bangladesh Council of Scientific and Industrial Research (BCSIR), Dhaka 1000, Bangladesh

Abstract

In this paper, the study of research on the microstructure and corrosion behavior and mechanical properties of a Mg-5.45Zn-6.63Sn-0.51Ca alloy under different thermal and mechanical states is reported. The cast of the alloy in a mild steel mould took place at 700°C; then, it was homogenized at 400°C for 18 hours and characterized by means of optical microscopy, X-ray diffraction, and scanning electron microscopy. The corrosion behavior was tested in the 3.5% NaCl solution using corrosion potential and linear polarization resistance (LPR) measurements. Post-corrosion analysis of the degraded surface was carried out by SEM. After that, the samples were hot-rolled at 400°C down to 15% of their original thickness and again tested. It was therefore concluded that hot rolling had a major microstructural influence on the properties, an observation consistent with comparison between results in the homogenized and rolled conditions. Hot Rolling tends to improve the corrosion resistance of the alloy and refines the microstructure. Tensile strength, and elongation at failure were obtained using tensile tests, carried out on the hot-rolled samples at temperatures ranging from 200 to 350°C, and two strain rates of 10^{-4} and 5×10^{-4} s^{-1}.

Keywords: *Mg-Zn-Sn-Ca alloy; Corrosion Resistance; High Temperature Mechanical Properties.*

Introduction

Research in magnesium alloys has become very intense in the recent past because of their lightweight property and possible application in the automotive and aerospace industry. Most of the magnesium alloys are recognized for their high strength-to-weight ratio, which bears much importance for fuel saving and low emission in transportation. On these lines, the magnesium alloys containing zinc (Zn), tin (Sn), and calcium (Ca), are unique in nature because of their peculiar mechanical and corrosion properties. The other element that is quite famous for making the Mg alloy system proper in the mechanical properties with resistance against corrosion is Zn and Sn, when added. The addition of Zn and Sn increases strength and ductility for Mg, whereas addition of Ca further improves its mechanical performance and corrosion resistance. Earlier studies have shown that the addition of minor elements in Mg-Zn-Sn alloys, such as Al and Mn, can refine the grain structure to a great extent and improve the mechanical properties [1][2]. The microstructural characteristics of magnesium-based alloys play a very important role in determining both their mechanical properties and corrosion behavior. For instance, the presence of second-phase particles and solute content in the matrix have shown an influence on the

*Corresponding author: mdnahidrahman.mme.buet@gmail.com

corrosion rate of Mg-Sn-Zn alloys in immersion and salt spray environments [3]. Other factors that can influence behavior under deformation, such as the grain size and texture of the magnesium alloy, are reported for hot-rolled magnesium sheets showing orthotropic behavior [4]. Corrosion resistance is one of the most important factors to the practical application of magnesium alloys, especially in environments like 3.5 wt % NaCl solutions simulating marine conditions. A variety of surface treatments and alloying strategies are being studied to improve the corrosion resistance of magnesium alloys.

For example, surface remelting treatments enhance the corrosion resistance of AZ91 magnesium alloys through grain structure refinement and β-$Mg_{17}Al_{12}$ phase distribution control [5]. In addition, it has been reported that the addition of minor rare-earth elements, for example cerium, also results in increased resistance of magnesium anodes to corrosive attacks in the electrolyte used [6].

This work examines the microstructure, corrosion performance, and mechanical properties of the new Mg-5.45Zn-6.63Sn-0.51Ca alloy.

Experimental Procedure

I. Alloy Casting: The Mg-5.45Zn-6.63Sn-0.51Ca (wt%) alloy was prepared using high-purity Mg, Zn, Sn, and Ca. The alloy was cast in an argon environment, with the constituents melted in a preheated mild steel mould at 700°C using an induction furnace. The alloy was then poured into the mould at the same temperature followed by air cooling.

II. Homogenization: The cast alloy was subjected to homogenization at 400°C for 18 hours. This process was conducted in a resistance furnace under an air atmosphere.

III. Hot Rolling Process: The homogenized samples were hot rolled at 400°C with a 15% reduction in thickness. The rolling was carried out in multiple passes.

IV. Materials Characterization:

- X-ray Fluorescence (XRF): XRF was carried out in the as cast sample to find out the actual composition of elements present in the alloy.
- Optical Microscopy: The homogenized and rolled samples were polished and etched using an 2% Nital solution. Optical microscopy was performed at various magnifications to observe the microstructure.
- X-Ray Diffraction (XRD): XRD analysis was conducted to identify the phases present in the homogenized and rolled samples. The scans were performed using Cu-Kα radiation.
- Scanning Electron Microscopy (SEM): SEM coupled with Energy Dispersive X-ray Spectroscopy (EDS) was employed to analyze the microstructure and identify secondary phases in the homogenized and rolled samples.

V. Corrosion Performance Testing:

- Corrosion Potential Measurement: The corrosion potential (E_{corr}) was recorded using a standard three-electrode setup (Calomel electrode as reference electrode and Pt electrode as counter electrode) in a 3.5% NaCl solution for both homogenized and rolled samples in *Gamry Instruments Reference 3000* potentiostat.
- Linear Polarization Resistance (LPR): LPR tests were conducted to evaluate the corrosion resistance by measuring the Polarization Resistance (Rp), Open Circuit Potential (OCP) of the alloy in the homogenized and rolled conditions using the same solution that was used in corrosion potential measurement in *Gamry Instruments Reference 3000* potentiostat.
- Post-Corrosion SEM: After the LPR test, the corroded surfaces were examined using SEM to study the morphology and distribution of corrosion products.

VI. Tensile Testing of Hot Rolled Samples: Tensile tests on hot-rolled samples were conducted at 200°C, 250°C, 300°C, and 350°C, with strain rates of 10^{-4} and 5×10^{-4} s^{-1}. Tensile strength, and elongation at failure were recorded in Testometric Materials Testing Machine-X500.

Results and Discussions

X-ray Fluorescence (XRF)

The composition of the alloy is listed in Table 1.

Table 1. Composition of the alloy

Elements	Zn	Sn	Ca	Mg
Composition (wt%)	5.45	6.63	0.51	Balance

Optical Microstructure

Fig. 1 contains the microstructure of the alloy both in homogenized and rolled condition at different magnifications.

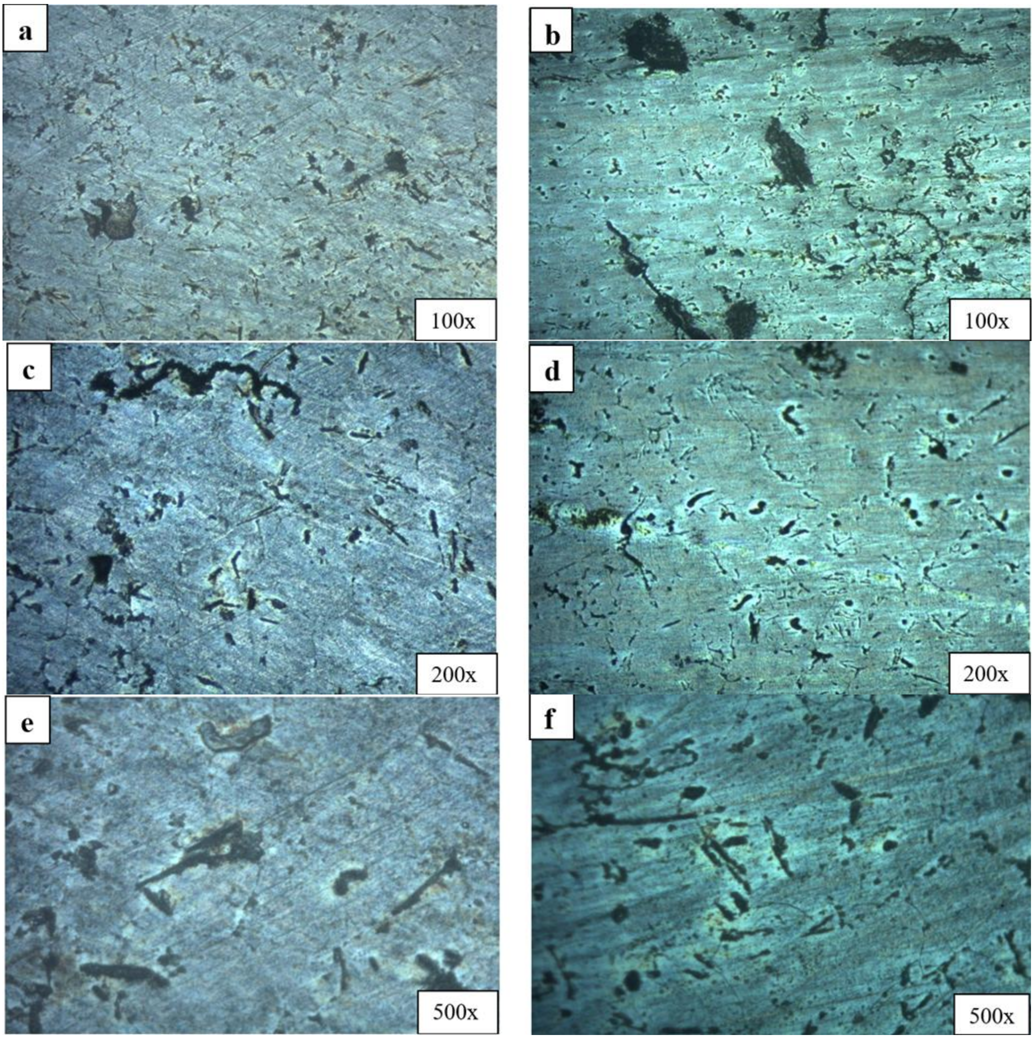

Fig. 1. Optical Microstructure of the alloy [a, c, e (Left) is in Homogenized Condition and b, d, f (Right) is in Rolled Condition]

The microstructure of the homogenized sample consists of a typical, even distribution of phases with minimal grain boundaries, while the rolled sample indicated an elongated grain with increased evidence of grain boundaries due to deformation from the rolling process. Such transformation from equiaxed grains in the homogenized state to elongated grains in the rolled state has been well documented. Precipitates in the homogenized samples are randomly distributed while rolling causes their alignment. According to Ikeda et al., and Yu et al., similar microstructural changes have been observed in previous works concerning Mg alloys; homogenization caused the uniformity of the phase distribution, while rolling generated deformation textures and grain refinement [7][8]. The micrograph shows porosity distributed in a more uniform way in the homogenized sample; rolling causes alignment of the pores.

Volume Fraction of Porosity

The volume fraction of porosity in the alloy was estimated using the very common open-source ImageJ program. The obtained values are given in Table 2.

Table 2. Percent Porosity of the alloy for Homogenized and Rolled condition

Condition	Porosity (%)
Homogenized	4.921
Rolled	2.424

Porosity was higher for the homogenized condition, being 4.921%, while for the rolled condition it was lower, amounting to 2.424%. The literature reports such reduction of porosity for the material after rolling; according to Zhao et al., hot rolling has been stated as a means of decreasing the porosity of metallic alloy by closing the voids in the material, with a related increase in density [9]. According to Kittner et al., Dynamic recrystallization during hot rolling of magnesium, diminishes porosity compared to other working conditions [10].

X-Ray Diffraction (XRD) Analysis

Figure 2 shows the X-Ray Diffraction pattern of the Mg-5.45 Zn-6.63 Sn-0.51 Ca alloy in both the homogenized and rolled conditions, highlighting the presence of Magnesium (α-Mg), Magnesium Stannide (Mg_2Sn), Calcium Magnesium Zinc ($Ca_2Mg_6Zn_3$), and Calcium Magnesium Stannide (CaMgSn), exhibits distinct phases and corresponding crystal planes.

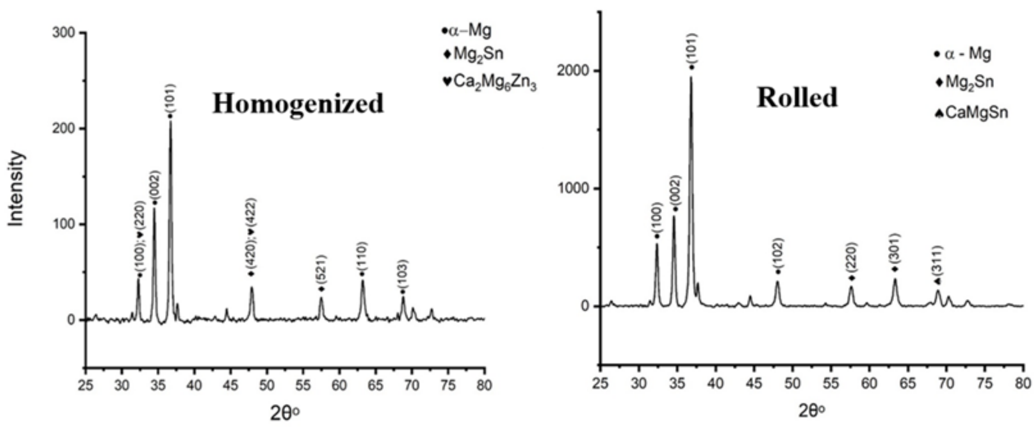

Fig. 2. XRD results of Mg- 5.45 Zn- 6.63 Sn- 0.51 Ca alloy in Homogenized and Rolled conditions

In the homogenized state, the alloy primarily shows peaks for magnesium (α-Mg), which according to Mondet et al., align with a hexagonal close-packed structure, as indicated by peaks at 32.2°, 34.4°, 36.6°, 63.2°, and 69.2°, corresponding to the (100), (002), (101), (110), and (103) planes [11]. Additionally, peaks at 47.1° and 57.4° are associated with the (420) and (521) planes confirm the presence of the Mg_2Sn phase, according to Gabalcová et al, and Bovand et al., this phase contributes to an increased corrosion rate in chloride-rich environments due to galvanic corrosion [12][13]. Peaks corresponding to the $Ca_2Mg_6Zn_3$ phase are also observed, with the 32.2° and 47.1° peaks assigned to the (220) and (422) planes, according to Le et al., $Ca_2Mg_6Zn_3$ phase refines the microstructure, particularly when calcium (Ca) is added to the alloy [14] which has been shown to improve both mechanical properties and corrosion resistance according to Wang et al [15].

In the hot-rolled condition, the XRD pattern remains similar to the homogenized state, with prominent α-Mg and Mg_2Sn phases. The Mg phase is observed at 2θ values of 32.2°, 34.4°, 36.6°, and 47.5°, corresponding to the (100), (002), (101), and (102) planes. Peaks at 57.5° and 63.5° are attributed to the Mg_2Sn phase (220 and 301 planes). Notably, the hot-rolled alloy features the CaMgSn phase, according Zha et al., which forms during hot rolling, with a peak at 69.5° corresponding to the (311) plane [16], is absent in the homogenized condition. According to Zhang et al., CaMgSn plays a critical role in refining grain size, improving mechanical properties like microhardness and compressive yield strength [17].

SEM Observation with EDS

Figure 3 shows the SEM images of the alloy in homogenized condition and rolled condition for low and high magnifications.

In homogenized condition micrograph (a) shows the microstructure with fine grains; some precipitates are distinguishable. In (b), the grain structure is seen in a wider view, demonstrating the relatively uniform distribution. Both images give evidence for secondary phases or precipitates that could be Zn-rich or Sn-rich, since these elements are important in the composition, as confirmed by XRD analysis.

Homogenization at 400°C normally dissolves second-phase particles for uniform grain structure. However, from the images obtained, it was observed that some second-phase particles still remained; nonetheless, most of the alloying elements were relatively uniformly distributed just like in other Mg alloys. According to Kulkarni et al., dissolution kinetics of γ-$Mg_{17}Al_{12}$ phase in the AZ80 magnesium alloy, homogenization at 400°C resulted in its partial dissolution, ductility improvement, and a more homogeneous microstructure with a few secondary-phase particles [18]. The microcracks or porosity represented in image (a) most likely developed during the homogenization process or as a casting defect. Andrzej Kielbus et al., pointed out that this type of defect may serve as a stress concentrator, affecting the mechanical properties of the alloy [19].

In rolled condition, high-magnification SEM image (c) shows elongated second-phase particles, probably intermetallic compounds of Zn, Sn and Ca, which are aligned in the rolling direction with a uniformly grained magnesium alloy matrix. Thus, dynamic recrystallization is suggested to have happened during rolling. The lower-magnification image (d) shows a smooth surface with fine and evenly dispersed particles.

According to Javaid et al., hot rolling above 300°C facilitates dynamic recrystallization and thus generates a uniform, fine-grained microstructure [20]. Deng et al., pointed that SEM observations of Mg alloys after hot rolling generally reveal equiaxed grains with a smaller number of dislocations, thus resulting in a more stable, ductile alloy with better corrosion resistance [21].

Fig. 4 and Table 3 summarizes the EDS results of Mg- 5.45Zn- 6.63Sn- 0.51Ca alloy in homogenized and rolled condition.

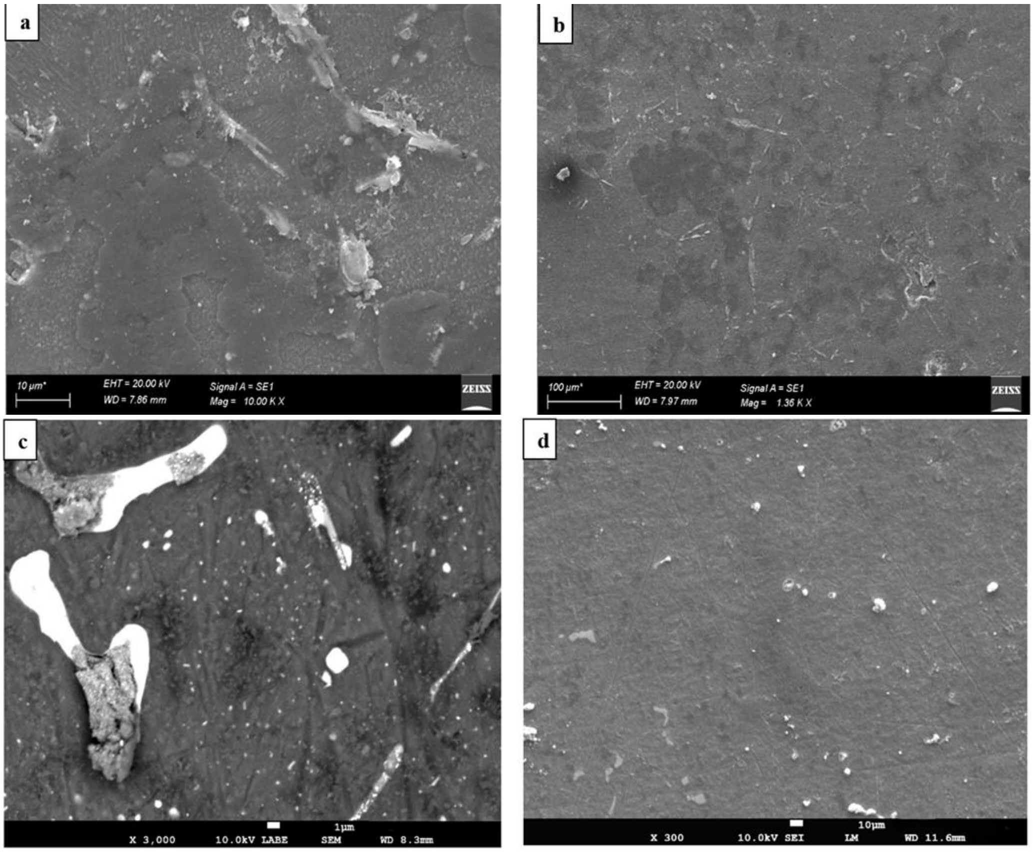

Fig. 3. SEM images of alloy at homogenized condition (a) high magnification (b) low magnification and rolled condition (c) high magnification (d) low magnification

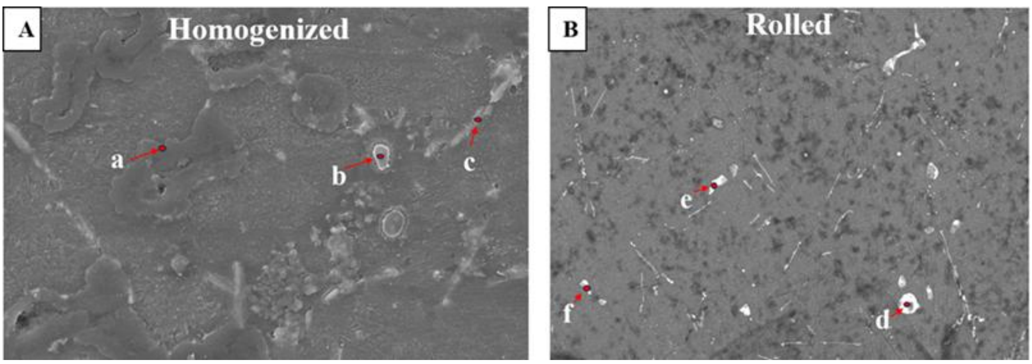

Fig. 4. SEM image of the alloy for EDS analysis (A) Homogenized (B) Rolled condition

The phase transformations identified in this study clearly demonstrate the combined effect of thermal and mechanical treatments on alloy microstructures. Homogenization primarily resulted in oxidation and some intermetallic formation, while rolling further diversified the phase composition by enhancing diffusion and mechanical mixing.

Size Distribution and Volume Fraction of Secondary Phase Particle

Particle size distribution and volume fraction of secondary phase particle were measured by using ImageJ software and analysed for the alloy in Fig. 5 and Table 4 for homogenized and rolled condition respectively.

Table 3. EDS results of Mg- 5.45Zn- 6.63Sn- 0.51Ca in Homogenized and rolled condition

Condition	Position	Mg (at%)	Zn (at%)	Sn (at%)	Ca (at%)	O (at%)	Phase
Homogenized	a	36.75	-	-	-	63.25	MgO (highly oxidized)
	b	66.44	-	-	-	32.56	MgO (less oxidized)
	c	62.39	-	3.97	-	33.64	Mg_2SnO_4
Rolled	d	31.71	0.19	13.60	2.77	51.73	MgO, Mg_2Sn
	e	37.79	0.39	17.64	3.11	40.87	MgO, CaMgSn
	f	59.57	1.44	9.91	2.00	27.08	MgO, Mg_2Ca

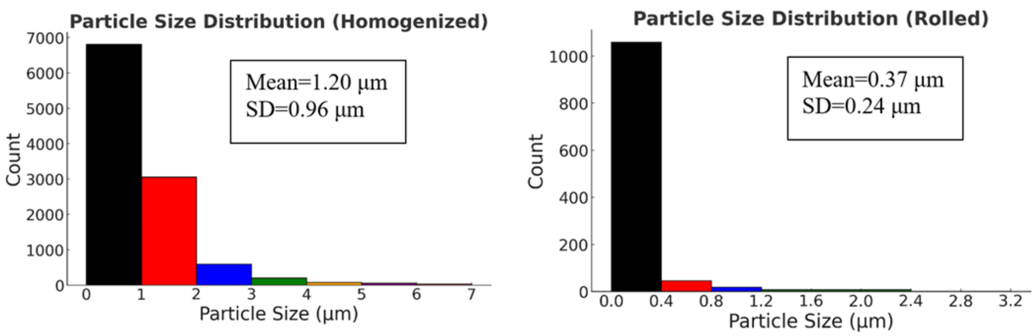

Fig. 5. Particle Size Distribution of the alloy

The particle size of homogenized sample was found to be approximately 1.20 µm (with a standard deviation of 0.96 µm) and for rolled sample the mean was approximately 0.37 µm (with a standard deviation of 0.24 µm). The average particle size was reduced from approximately 1.20 µm in the homogenized sample to around 0.37 µm in the rolled sample. From Vinogradov et al., and Liu et al., this reduction is consistent with the expected effects of plastic deformation processes like rolling, which typically refine the microstructure by breaking down larger particles and distributing them more uniformly [22] [23].

Table 4. Volume Fraction of Secondary Phases in the alloy for Homogenized and Rolled condition

Condition	Volume Fraction of Secondary Phases (%)
Homogenized	6.18
Rolled	2.21

Volume fraction of secondary phase particle for homogenized condition is 6.18% and for rolled condition it is 2.21% respectively. So, it is a clear indication that, hot rolling at 400^{o}C results in a reduction of secondary phase particle. Hot rolling involves mechanical and thermal effects that promote dynamic recrystallization and the dissolution of secondary phase particles. According to Guo et al., in, Al–Si–Fe–Mg alloys hot rolling was found to break down eutectic phases and redistribute them more uniformly, leading to refined particles [24]. This suggests that the mechanical action during rolling effectively reduces and redistributes secondary phases.

Corrosion Behavior Analysis

Corrosion Potential as a function of Time

Fig. 6 shows the Corrosion Potential (E_{corr}) curve of Mg- 5.45Zn- 6.63Sn- 0.51Ca alloy in homogenized and rolled condition. Table 5 summarizes the findings.

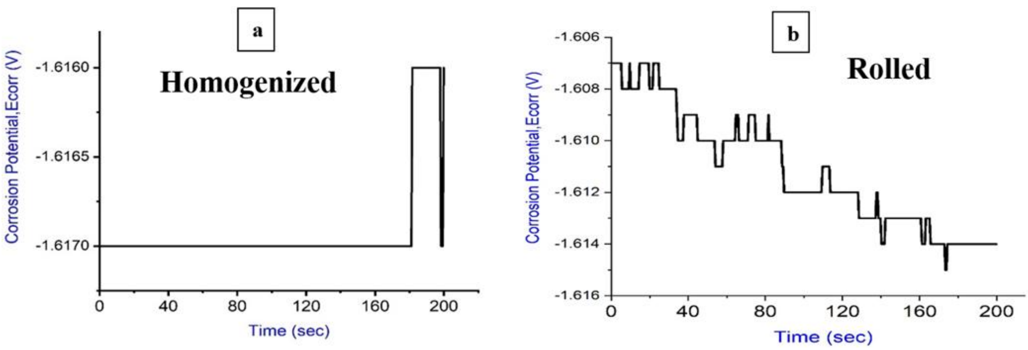

Fig. 6. Corrosion Potential as a function of Time for the Alloy in (a)Homogenized and (b)Rolled Condition in 3.5% NaCl solution.

The rolled sample exhibits a more positive corrosion potential range (-1.615 V to -1.607 V) compared to the homogenized sample (-1.617 V to -1.616 V). According to Xiang et al., and Sun et al., a more positive E_{corr} typically suggests better corrosion resistance [25][26]. As seen in the analysis of Ghorbani et al. and Zhang et al., despite more fluctuation, the curve of the rolled sample maintained a higher potential generally, reflecting more stable passive layer formation over time, compared with the homogenized sample, which shows a sudden drop, hence less stable corrosion resistance [27][28].

Table 5. Corrosion Potential of the Alloy in Homogenized and Rolled Condition in 3.5% NaCl solution

Condition	E_{corr} (V)	
	Min	Max
Homogenized	-1.617	-1.616
Rolled	-1.615	-1.607

Open Circuit Potential

Fig. 7 shows the Open Circuit Potential (OCP) curve of the alloy in homogenized and rolled condition.

According to Choudhary et al., the more positive the OCP, the better its corrosion resistance, which is related to nobler behavior in the electrochemical series [29]. From these OCP values, it can be said that the rolled sample will have more corrosion resistance compared to the homogenized sample because its OCP value (-1.614 V) is more positive than the OCP value of the homogenized sample (-1.622 V).

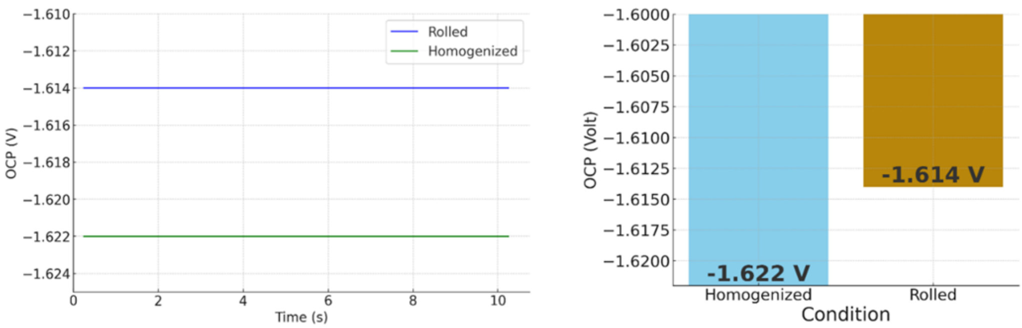

Fig. 7. Open Circuit Potential (OCP) for the alloy in homogenized and rolled condition in 3.5% NaCl solution

Linear Polarization Resistance

Fig. 8 shows the Linear Polarization Resistance curve of Mg- 5.45Zn- 6.63Sn- 0.51Ca alloy in homogenized and rolled condition.

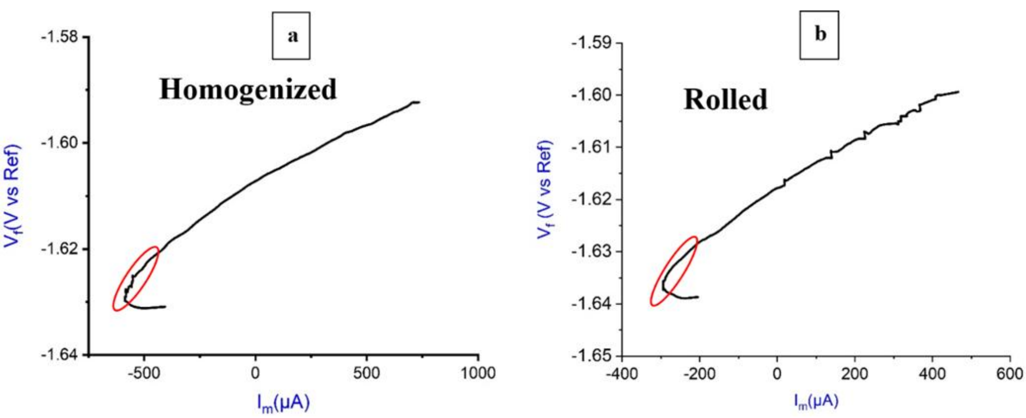

Fig. 8: Linear Polarization Resistance (LPR) curve for the alloy in (a)Homogenized and (b)Rolled Condition in 3.5% NaCl solution

The rolled condition shows a lower current (147.3 µA) than the homogenized condition (307.8 µA), suggesting a slower corrosion rate which is also confirmed from their corrosion rate (421.7 mpy for rolled sample and 890.4 mpy for homogenized sample). Kumrular et al., stated, higher Polarization Resistance (Rp) values generally indicate better corrosion resistance [31]. The rolled sample has a much higher polarization resistance (176.9 ohms) compared to the homogenized sample (84.1 ohms), indicating superior performance.

Table 6. Corrosion Potential (E_{corr}), Corrosion Current (I_{corr}), Polarization Resistance (R_p) and Corrosion Rate (mpy) of the Alloy in the Red marked region from Linear Polarization Resistance test in 3.5% NaCl solution for Homogenized and Rolled condition

Condition	E_{corr} (V)	I_{corr} (µA)	R_p (ohm)	Corrosion Rate (mpy)
Homogenized	-1.618	307.8	84.1	890.4
Rolled	-1.607	147.3	176.9	421.7

SEM and EDS Observation of Corroded Surface

Figure 9 shows the SEM images of corroded surface in homogenized and rolled condition for low and high magnifications.

The analysis of scanning electron microscopy (SEM) images shows a broken and rough surface morphology, which is an indicative sign of corrosion processes in magnesium alloys. This morphology corresponds to the corrosion products that are produced and the degradation of the alloy surface. According to Jiang et al., cracks in the surface suggest that it was subjected to significant stress, possibly from corrosion products forming and then swelling or contracting as they expand on their own [32].

Fig. 10 and Table 7 summarizes the EDS results of Mg- 5.45Zn- 6.63Sn- 0.51Ca alloy's corroded surface in homogenized and rolled condition.

Elemental analysis reveals a significant oxygen content, between 72 and 77 atom%, representing the occurrence of oxides or hydroxides as the deposits after corrosion. This is typical of magnesium alloys in chloride-containing environments. The presence of magnesium, at 24–26 atom% in surface composition, confirms it as a main alloy element that remains after corrosion. According to Song et al., the detection of chlorine, at 0.8-3.0 atom%, in the alloy indicates that chloride ions from moist NaCl solution attacked the alloy, forming pits and localized corrosion [33]. It has been speculated that the high oxygen content, combined with the presence of magnesium and chlorine, establishes a typical pitting corrosion mechanism for this alloy within a chloride environment [33]. According to Wei et al., initially, the magnesium oxide and hydroxide formed may act as a harmless layer. However, if this layer has cracks, it reduces its effectiveness over time. When chloride ions attack and interfere with this protective layer, severe corrosion occurs [34].

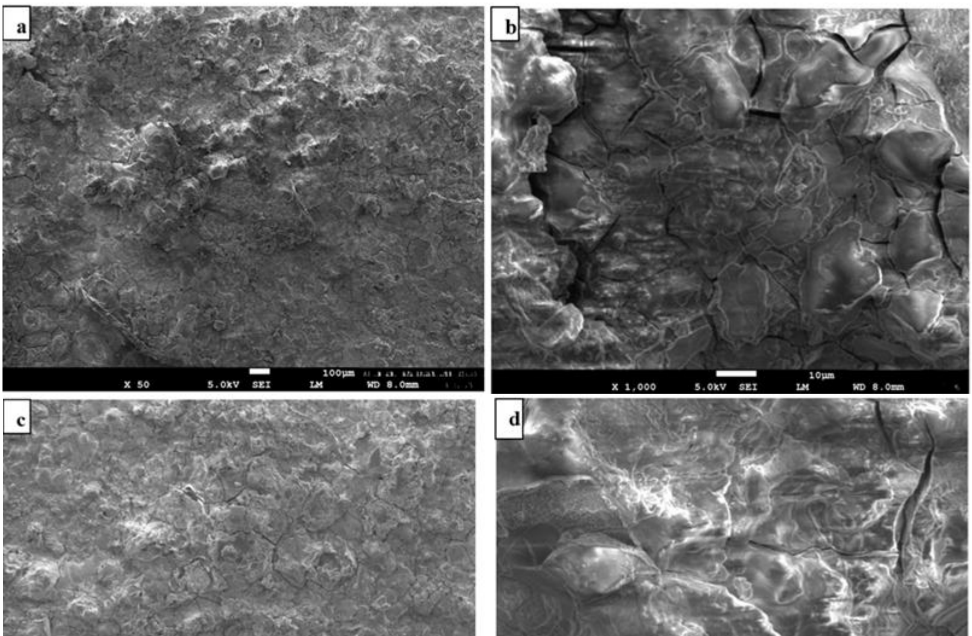

Fig. 9. SEM images of corroded surface at homogenized condition (a) low magnification (b) high magnification and rolled condition (c) low magnification (d) high magnification

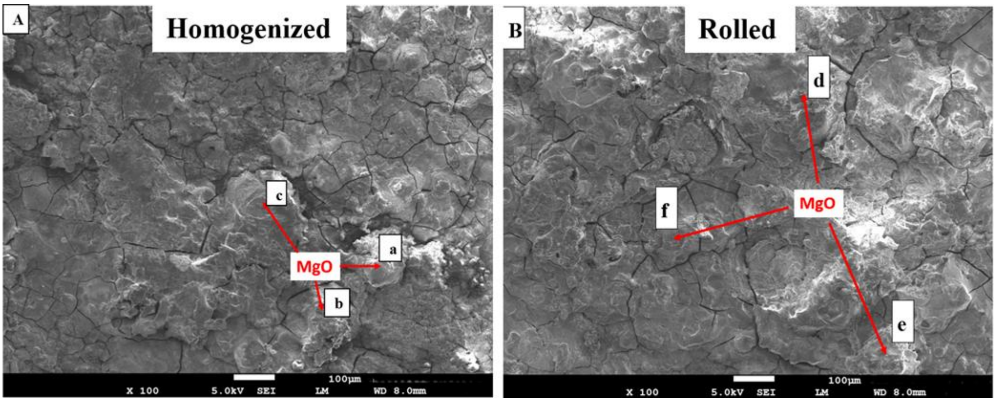

Fig. 10. SEM images of the alloy's corroded surface for EDS analysis (A) Homogenized (B) Rolled condition.

Table 7. EDS results of corroded surfaces of Mg- 5.45Zn- 6.63Sn- 0.51Ca in Homogenized and rolled condition

Condition	Position	Mg (at%)	Zn (at%)	Sn (at%)	Ca (at%)	O (at%)	Cl (at%)
	a	25.57	0.03	-	0.18	72.55	1.68
Homogenized	b	24.90	0.08	0.03	-	74.72	0.28
	c	24.17	0.03	-	-	74.92	0.88
	d	22.96	0.09	0.01	-	76.46	0.46
Rolled	e	22.73	0.16	-	0.17	73.92	3.02
	f	24.62	0.08	-	0.21	74.94	0.15

High Temperature Mechanical Performance Evaluation

The high temperature mechanical properties of the alloy for rolled condition was evaluated through eight tensile tests at 200°C, 250°C, 300°C and 350°C for 10^{-4} and 5×10^{-4} s^{-1} strain rates. The resulted curves and values are given in Fig. 11 and Table 8.

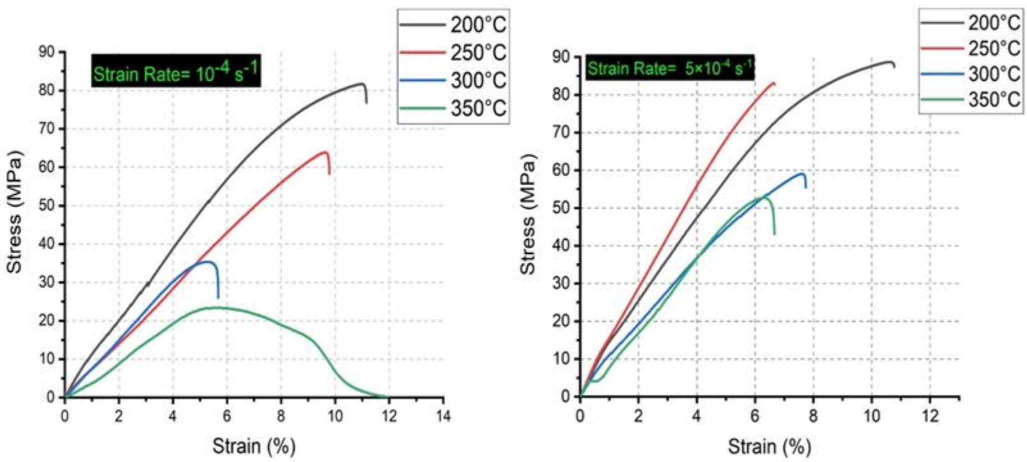

Fig. 11. Engineering Stress-Strain Curves for (a) Low and (b) High Strain Rates at Different Temperatures.

The obtained results of the experimental tests point out the obvious trend of reducing tensile strength of the tested material with the rise of temperature within the tested strain rates. The tensile strength is reduced from 81.66 MPa at 200°C to 23.42 MPa at 350°C at the strain rate of 10^{-4} s^{-1}. This result confirms the literature information of Zhang et al., which has established that at high temperatures, the mechanical strength of magnesium alloys is low [35]. According to Chai et al., this is principally a result of the thermally activated softening mechanisms of dynamic recrystallization and grain boundary sliding, strength is lost because the degrading alloy microstructure at an elevated temperature reduces the resistance for the movement of dislocations [36].

Table 8. Tensile Strength and Elongation at Failure for different temperatures and strain rates

Strain Rate (s^{-1})	Temperature(°C)	Tensile Strength (MPa)	Elongation at Failure (%)
10^{-4}	200	81.66	11.16
	250	63.87	9.78
	300	35.34	5.67
	350	23.42	11.98
5×10^{-4}	200	88.75	10.82
	250	83.07	6.67
	300	59.06	7.74
	350	52.95	6.67

Mostly, the elongation at failure increases with the rise of temperature up to a maximum before falling again with the further increase in temperature, as in data for 10^{-4} s^{-1}, where the elongation increases from 11.16% at 200°C to 11.98% at 350°C. Indeed, this is the general trend in the magnesium alloy, since higher temperatures enhance ductility through processes such as dynamic recovery and recrystallization [35]. The elongation falls beyond these temperatures because of grain boundary weakening and probable melting or softening near the melting point.

In general, the tensile strength is higher at higher strain rates than at the lower-strained ones. This will be demonstrated by the examples: the tensile strengths at 200°C increase from 81.66 MPa up to 88.75 MPa with the increase in the strain rates from 10^{-4} s^{-1} to 5×10^{-4} s^{-1}. According to Ang et al., and Noradila et al., this is typical for magnesium alloys because their single crystal structure of HCP restricts the propagation of dislocations, hence leading to strong work hardening at higher strain rates [37] [38]. The increase of the flow stress with increasing strain rate is attributed to the limited time available for dislocation motion and dynamic recovery processes [36]. This alloy has a very slight increase in ductility with reduced strain rate. More specifically, the ductility or elongation decreases slightly from 11.16% to 10.32% at 200°C while the strain rate is increased from 10^{-4} s^{-1} to 5×10^{-4} s^{-1}. While the time for dynamic recovery processes such as recrystallization is reduced at the higher strain rates, the reduction in ductility is only slight [36].

Conclusions

From this research, major microstructural, mechanical, and corrosion resistance insights emerged under different thermal and mechanical treatments for the Mg-5.45Zn-6.63Sn-0.51Ca alloy. The alloy's microstructure in the homogenization state displayed evenly distributed phases with few grain boundaries; the rolled condition, distance-across-grain-poled, showed an increased number of grain boundaries along with aligned secondary phase particles. Rolling at 400°C fine-tuned the microstructure from a particle size of 1.20 μm down to 0.37 μm, while the volume fraction of the secondary phases dropped from 6.18% to 2.21%. Homogenized specimens were found to be more porous (4.921%) than the rolled specimens (2.424%), implicating that rolling has closed down the voids and augmented dynamic recrystallization. X-ray diffraction (XRD) study revealed the presence of α-Mg and Mg_2Sn phases in both states, while rolling introduced the beneficial CaMgSn phase that contributed to improved grain refinement and mechanical strength.

Mechanically, the alloy showed decreased tensile strength as the temperature increases, consistent with thermally activated softening in Mg alloys. At a strain rate of 10^{-4} s^{-1}, tensile strength dropped from 81.66 MPa at 200°C to 23.42 MPa at 350°C. Higher strain rates led to increased tensile strength with a little loss of ductility because of inhibited dislocation movement.

Testing for corrosion performance showed rolling specimens performed better with a higher (less negative) corrosion potential and a reduced corrosion rate of 421.7 mpy in comparison with 890.4 mpy for the homogenized condition. Again, the polarization resistances of the rolled specimens (176.9 ohm) were higher than for the homogenized specimens, pointing at their enhanced corrosion resistances. The SEM analysis of the corroded surfaces showed that rolled samples provided much milder corrosion damage, and through the elemental analysis, it was found that such treatments induced the formation of protective oxide layers that positively contributed to the corrosion resistance, hence allowing for localized corrosion when cracks in these layers developed.

The results indicate that a combined effect of homogenization followed by hot rolling at 400°C optimizes microstructural characteristics, which in turn improves corrosion resistance. The formation of such phrases as CaMgSn is crucial in microstructural refinement and thus, for improved properties. Controlled thermal and mechanical processing would significantly benefit magnesium alloys for such high-performance applications that require lightweight properties and durability; this can be seen in the automotive and aerospace sectors.

Acknowledgment

The authors acknowledge the funding the Bangladesh University of Engineering and Technology provided under ‘Research Projects Under Higher Training & Research Program’, CASR Meeting No 354, Resolution No. 79, dated 16 June 2022. The author also thanks the Bangladesh Council of Scientific and Industrial Research (BCSIR) for allowing the use of equipment during the study. Materials were obtained through the GARE project of the Ministry of Education, Government of Bangladesh.

References

[1] Yan, S., Hou, C., Zhang, A. and Qi, F., 2023. *Influence of Al Addition on the Microstructure and Mechanical Properties of Mg-Zn-Sn-Mn-Ca Alloys*. **Materials, *16*(10)**, p.3664.

[2] Hou, C., Qi, F., Ye, Z., Zhao, N., Zhang, D. and Ouyang, X., 2020. *Effects of Mn addition on the microstructure and mechanical properties of Mg–Zn–Sn alloys*. **Materials Science and Engineering*: A***, *774*, p.138933.

[3] Woo, S.K., Yim, C.D., Kim, H.S. and You, B.S., 2016. *Effects of Microstructural Factors on Corrosion Behavior of As-Extruded Mg-Sn-Zn Alloys in Immersion and Salt Spray Environments.* ***Corrosion*, *72*(9)**, pp.1146-1154.

[4] Ullmann, M., Kaden, C., Kittner, K. and Prahl, U., 2022. *Orthotropic behavior of twin-roll-cast and hot-rolled magnesium ZAX210 sheet.* **Materials, 15(18)**, p.6437.

[5] Iwaszko, J. and Strzelecka, M., 2022. *Microstructure and Corrosion Resistance of AZ91 Magnesium Alloy after Surface Remelting Treatment*. **Materials, 15(24),** p.8980.

[6] Li, X., Gao, S., Liu, Q., Gao, J., Yan, Z., Liu, M., Liu, S. and Wang, E., 2023. *The solute cerium to enhance corrosion resistance of magnesium anode in 3.5% NaCl solution*. **Ionics, 29(5),** pp.1923-1933.

[7] Ikeda, K.I., Takashita, T., Akiyoshi, R., Hata, S., Nakashima, H., Yamada, K. and Kaneko, K., 2018. *Effects of Scandium and Zirconium Addition on Recrystallization Behavior of Al–Mg–Si Alloy.* **Materials Transactions, 59(4),** pp.590-597.

[8] Yu, R.C., Liu, Z.Y., Liu, Y.B., Xu, M., Yan, K. and Ma, F.Y., 2006. *Hot working process of a high strength heat resisting Al-Cu-Mg-Ag alloy.* **Heat Treatment of Metals (China), 31(5),** pp.75-79.

[9] Zhao, Y., Jin, Y. and Bao, Y., 2023. *Effect of process parameters on porosity defects in Al-Si alloy hot rolling.* **Proceedings of the Institution of Mechanical Engineers, Part B: Journal of Engineering Manufacture, 237(5),** pp.770-778.

[10] Kittner, K., Ullmann, M. and Prahl, U., 2022. *Microstructural and Textural Investigation of an Mg-Zn-Al-Ca Alloy after Hot Plane Strain Compression.* **Materials, 15(21)**, p.7499.

[11] Mondet, M., Barraud, E., Lemonnier, S., Guyon, J., Allain, N. and Grosdidier, T., 2016. *Microstructure and mechanical properties of AZ91 magnesium alloy developed by Spark Plasma Sintering.* **Acta Materialia, 119**, pp.55-67.

[12] Gabalcová, Z., Gogola, P., Gerhátová, Ž. and Palcut, M., 2022. *Corrosion behavior of an Mg2Sn alloy*. **Materials, 15(6)**, p.2025.

[13] Bovand, D., Abdollah-Pour, H., Mirzaee, O. and Bagherifard, S., 2022. *Dry sliding wear and corrosion performance of Mg-Sn-Ti alloys produced by casting and extrusion*. **Materials, 15(10)**, p.3533.

[14] Le, T., Mao, P., Hu, W. and Le, Q., 2024. *Effects of Zn/Ca Alloying on the Second Phase, Corrosion Behavior, and Mg–Air Battery Anodic Performance of Mg–1Sn-Based Alloys.* **Advanced Engineering Materials, 26(6)**, p.2301130.

[15] Wang, L., Li, J.B., Li, L., Nie, K.B., Zhang, J.S., Yang, C.W., Yan, P.W., Liu, Y.P. and Xu, C.X., 2017. *Microstructure, mechanical and bio-corrosion properties of Mg–Zn–Zr alloys with minor Ca addition.* **Materials Science and Technology, 33(1)**, pp.9-16.

[16] Zha, M., Liang, J.W., Xing, H., Xu, H., Jiang, B., Wang, C., Jia, H.L. and Wang, H.Y., 2022. *Spheroiding and refining of coarse CaMgSn phase in Mg–Al–Sn–Ca alloys for simultaneously improved strength and ductility via sub-rapid solidification and controlled rolling.* **Materials Science and Engineering: A, 834**, p.142598.

[17] Zhang, J., Zhou, G., Jiang, B., Luo, A., Zhao, X., Tang, A. and Pan, F., 2021. *A Novel Mg–CaMgSn Master Alloy for Grain Refinement in Mg–Al-Based Alloys.* **Metals, 11(11)**, p.1722.

[18] Kulkarni, R.R., Prabhu, N., Hodgson, P.D. and Kashyap, B.P., 2014. *Kinetics of γ-Mg17Al12 phase dissolution and its effect on room temperature tensile properties in As-Cast AZ80 magnesium alloy.* **Solid State Phenomena, 209**, pp.207-211.

[19] Pikos, I., Kiełbus, A. and Adamiec, J., 2013. *The influence of casting defects on fatigue resistance of elektron 21 magnesium alloy.* **Archives of Foundry Engineering, 13(2)**, pp.103-106.

[20] Javaid, A. and Czerwinski, F., 2019. *Effect of hot rolling on microstructure and properties of the ZEK100 alloy.* **Journal of Magnesium and Alloys, 7(1)**, pp.27-37.

[21] Deng, B., Dai, Y., Lin, J. and Zhang, D., 2022. *Effect of rolling treatment on microstructure, mechanical properties, and corrosion properties of WE43 alloy*. **Materials, 15(11)**, p.3985.

[22] Vinogradov, A., Merson, E., Myagkikh, P., Linderov, M., Brilevsky, A. and Merson, D., 2023. *Attaining high functional performance in biodegradable Mg-alloys: an overview of challenges and prospects for the Mg-Zn-Ca system.* **Materials, 16(3)**, p.1324.

[23] Liu, G., Xu, J., Feng, B., Liu, J., Qi, D., Huang, W., Yang, P. and Zhang, S., 2022. *Comparison of corrosion performance of extruded and forged WE43 Mg alloy*. **Materials, 15(5**), p.1622.

[24] Guo, Y., Wang, Y., Jiang, B., Chen, H., Xu, H., Hu, M. and Ji, Z., 2022. *Microstructure evolution, thermal conductivity and mechanical properties of hot-rolling Al–Si–Fe–Mg alloy under different reductions*. **Modern Physics Letters B, 36(01)**, p.2150533.

[25] Xiang, P.E.N.G., SUN, J.W., LIU, H.J., WU, G.H. and LIU, W.C., 2022. *Microstructure and corrosion behavior of as-homogenized and as-extruded Mg− xLi− 3Al− 2Zn− 0.5 Y alloys (x= 4, 8, 12).* **Transactions of Nonferrous Metals Society of China, 32(1)**, pp.134-146.

[26] Sun, Y., Aydın, N.U., Turen, Y., Ahlatci, H. and Zengin, H., 2017. *Effect of Ti Addition on Corrosion Properties of As-Cast and Hot-Rolled AM60 Magnesium Alloys.* **Key Engineering Materials, 750,** pp.113-117.

[27] Ghorbani, F., Mirzadeh, H., Dehghanian, C. and Emamy, M., 2023. *Mechanical properties and corrosion behavior of biodegradable Mg–0.5 Zr–0.5 Ca–xZn magnesium alloys*. **Advanced Engineering Materials, 25(10)**, p.2201778.

[28] Zhang, C., Peng, C., Huang, J., Zhao, Y., Han, T., Wang, G., Wu, L. and Huang, G., 2022. *Investigation on microstructure and corrosion behavior of rolled Mg-1.5 Zn-xCa-xCe alloy.* **Anti-Corrosion Methods and Materials, 69(4),** pp.395-402.

[29] Choudhary, S., Garg, A. and Mondal, K., 2016. *Relation between open circuit potential and polarization resistance with rust and corrosion monitoring of mild steel*. **Journal of Materials Engineering and Performance, 25**, pp.2969-2976.

[30] Mayén, J., Hernández-Hernández, M., Del Carmen Gallegos-Melgar, A., Pereyra, I., Barredo, E., Abundez-Pliego, A. and Porcayo-Calderón, J., 2022. *Statistical analysis of corrosion current density and tensile strength of Al-6061 alloy by ageing and retrogression heat treatments*. **Transactions of the Indian Institute of Metals, 75(10)**, pp.2725-2735.

[31] Kumrular, B., Cicek, O., Dağ, İ.E., Avar, B. and Erener, H., 2023. *Evaluation of the corrosion resistance of different types of orthodontic fixed retention appliances: A preliminary laboratory study*. **Journal of Functional Biomaterials, 14(2)**, p.81.

[32] Jiang, J., Geng, X. and Zhang, X., 2023. *Stress corrosion cracking of magnesium alloys: A review.* **Journal of Magnesium and Alloys.**

[33] Song, G.L. and Atrens, A., 1999. *Corrosion mechanisms of magnesium alloys*. **Advanced engineering materials, 1(1)**, pp.11-33.

[34] Wei, L. and Gao, Z., 2023. *Recent research advances on corrosion mechanism and protection, and novel coating materials of magnesium alloys: a review.* **RSC advances, 13(12)**, pp.8427-8463.

[35] Zhang, L., Huang, Y., Wu, M., Xu, C., Ning, Z., Cao, F. and Sun, J., 2022. *Intermediate-Temperature Tensile Behavior of a Hot-Rolled Mg-Li-Al-Cd-Zn Alloy.* **Materials, 15(5)**, p.1686.

[36] Chai, F., Ma, Z., Han, X., Hu, X., Chang, Z. and Zhou, J., 2023. *Effect of strain rates on mechanical behavior, microstructure evolution and failure mechanism of extruded-annealed AZ91 magnesium alloy under room-temperature tension.* **Journal of Materials Research and Technology, 27**, pp.4644-4656.

[37] Ang, H.Q., Abbott, T.B., Zhu, S. and Easton, M., 2017. *Effect of strain rate on mechanical behavior of commercial die-cast magnesium alloys.* **Materials Science and Technology**.

[38] Noradila, A.L., Sajuri, Z., Syarif, J., Miyashita, Y. and Mutoh, Y., 2013, June. *Effect of strain rates on tensile and work hardening properties for Al-Zn magnesium alloys.* **IOP Conference Series: Materials Science and Engineering** (Vol. 46, No. 1, p. 012031). IOP Publishing.

Received: April 11, 2025
Accepted: May 22, 2025